Predicting Gait Patterns of Children With Spasticity by Simulating Hyperreflexia

Veerkamp, Kirsten; Carty, Christopher P.; Waterval, Niels F.J.; Geijtenbeek, Thomas; Buizer, Annemieke I.; Lloyd, David G.; Harlaar, Jaap; van der Krogt, Marjolein M.

DOI
10.1123/jab.2023-0022

Publication date
2023

Document Version
Final published version

Published in
Journal of Applied Biomechanics

Citation (APA)
Veerkamp, K., Carty, C. P., Waterval, N. F. J., Geijtenbeek, T., Buizer, A. I., Lloyd, D. G., Harlaar, J., & van der Krogt, M. M. (2023). Predicting Gait Patterns of Children With Spasticity by Simulating Hyperreflexia. *Journal of Applied Biomechanics*, *39*(5), 333-346. https://doi.org/10.1123/jab.2023-0022

Journal of Applied Biomechanics, 2023, 39, 334-346
https://doi.org/10.1123/jab.2023-0022

Human Kinetics
ORIGINAL RESEARCH

Predicting Gait Patterns of Children With Spasticity by Simulating Hyperreflexia

Kirsten Veerkamp,[1,2,3,4,5] Christopher P. Carty,[3,4,5,6] Niels F.J. Waterval,[1,2,7] Thomas Geijtenbeek,[8] Annemieke I. Buizer,[1,2,9] David G. Lloyd,[3,4,5] Jaap Harlaar,[8,10] and Marjolein M. van der Krogt[1,2]

[1]Department of Rehabilitation Medicine, Amsterdam UMC location Vrije Universiteit Amsterdam, Amsterdam, The Netherlands; [2]Rehabilitation & Development, Amsterdam Movement Sciences, Amsterdam, The Netherlands; [3]School of Health Sciences and Social Work, Griffith University, Gold Coast, QLD, Australia; [4]Griffith Centre of Biomedical & Rehabilitation Engineering (GCORE), Menzies Health Institute Queensland, Griffith University, Gold Coast, QLD, Australia; [5]Advanced Design and Prototyping Technologies Institute (ADAPT), Griffith University, Gold Coast, QLD, Australia; [6]Department of Orthopaedics, Children's Health Queensland Hospital and Health Service, Queensland Children's Hospital, Brisbane, QLD, Australia; [7]Department of Rehabilitation Medicine, Amsterdam UMC location University of Amsterdam, Amsterdam, The Netherlands; [8]Department of Biomechanical Engineering, Delft University of Technology, Delft, The Netherlands; [9]Emma Children's Hospital, Amsterdam UMC, University of Amsterdam, Amsterdam, The Netherlands; [10]Department of Orthopedics and Sports Medicine, Erasmus Medical Center, Rotterdam, The Netherlands

Spasticity is a common impairment within pediatric neuromusculoskeletal disorders. How spasticity contributes to gait deviations is important for treatment selection. Our aim was to evaluate the pathophysiological mechanisms underlying gait deviations seen in children with spasticity, using predictive simulations. A cluster analysis was performed to extract distinct gait patterns from experimental gait data of 17 children with spasticity to be used as comparative validation data. A forward dynamic simulation framework was employed to predict gait with either velocity- or force-based hyperreflexia. This framework entailed a generic musculoskeletal model controlled by reflexes and supraspinal drive, governed by a multiobjective cost function. Hyperreflexia values were optimized to enable the simulated gait to best match experimental gait patterns. Three experimental gait patterns were extracted: (1) increased knee flexion, (2) increased ankle plantar flexion, and (3) increased knee flexion and ankle plantar flexion when compared with typical gait. Overall, velocity-based hyperreflexia outperformed force-based hyperreflexia. The first gait pattern could mostly be explained by rectus femoris and hamstrings velocity-based hyperreflexia, the second by gastrocnemius velocity-based hyperreflexia, and the third by gastrocnemius, soleus, and hamstrings velocity-based hyperreflexia. This study shows how velocity-based hyperreflexia from specific muscles contributes to different spastic gait patterns, which may help in providing targeted treatment.

Keywords: predictive simulations, neuromusculoskeletal modeling, forward dynamics, spastic diplegia, cerebral palsy

Spasticity is a neural impairment affecting over 85% of children with cerebral palsy (CP).[1] CP is the most common childhood motor disorder, with an occurrence rate of around 2 in one thousand live births worldwide,[2] and is caused by injury to the developing brain during the perinatal period. In children, spasticity can also be a feature of hereditary spastic paraplegia, a group of rare genetic disorders, with a prevalence of 1.2 to 9.6 per 100,000.[3]

Spasticity is usually defined as a velocity-dependent increase of the muscle stretch reflex[4] and, therefore, is also known as stretch hyperreflexia.[5] This stretch hyperreflexia is caused by a lack of supraspinal suppression of the H-reflex[6] contributing to joint hyperresistance.[5] The combined impact of spasticity and other musculoskeletal impairments that often develop during growth results in a decline in gait function that adversely affects quality of life.[7]

Carty http://orcid.org/0000-0002-8969-5181
Waterval https://orcid.org/0000-0003-4025-7137
Geijtenbeek https://orcid.org/0000-0001-8352-8107
Buizer https://orcid.org/0000-0001-5662-2843
Lloyd https://orcid.org/0000-0002-0824-9682
Harlaar https://orcid.org/0000-0003-2889-271X
van der Krogt https://orcid.org/0000-0002-9219-7183
Veerkamp (k.veerkamp@amsterdamumc.nl) is corresponding author, https://orcid.org/0000-0003-2592-7059

Improving gait function is an important patient goal, and a range of treatments is available for spasticity management, including botulinum toxin type A injections and selective dorsal rhizotomy.[8,9] However, treatment selection is often difficult due to the presence of a combination of different neuromusculoskeletal impairments. When a child presents with a walking problem, it can be unclear what the most limiting impairment to that child's gait is, and, hence, what the most effective treatment would be. The cause and effect of how impairments like spasticity mechanistically affect gait are difficult to test experimentally as the impairments cannot be physically induced.

Instead, impairments can be induced in biocomputational models within predictive forward simulations, and, therefore, such simulations can be used to gain insight into causal mechanisms of which muscle impairments contribute to specific gait deviations. Doing so, the effects of plantar flexor weakness[10,11] and plantar flexor contracture[10,12] on gait were demonstrated. Spasticity has previously been modeled using stretch reflexes represented as velocity-dependent feedback controllers, which successfully estimated muscle behavior in fast stretches[13] and clinically reported deviations in spastic gait.[14,15] However, outcomes were not directly validated with experimental gait kinematics and kinetics. Recently, it was suggested that a force-related hyperreflexia model outperformed a velocity-based model when comparing each model's estimated muscle activity to experimental muscle activity during passive stretches and gait in children with spasticity.[16] This finding

is supported by a recent experimental study suggesting that muscle spindles encode force.[17] However, simulations were not fully predictive, limiting the evaluation of cause–effect mechanisms. A length-based mechanism has also been modeled as being involved in spasticity,[14,15] but it has been shown that most spastic muscles were only sensitive to length changes to a limited extent,[18] and increased length and velocity feedback were shown to result only in subtle temporal differences.[14] No previous studies have implemented force and velocity spasticity mechanisms into a predictive simulation workflow to predict gait of children with spasticity.

Therefore, the overall aim of this study was to model and compare these 2 hyperreflexia mechanisms in predictive simulations of gait to evaluate which mechanisms may underly gait deviations in children with spasticity. Two specific questions were addressed. First, does velocity- or force-based hyperreflexia better predict gait patterns in children with spasticity? Second, are different gait patterns in children with spasticity predicted by involvement of different muscles? Answering these questions could enhance understanding of how spasticity can contribute to gait deviations and which muscles may be important to treat when a child presents with a specific gait pattern.

Methods

Experimental Data Clusters

Data from 17 children with spastic paresis were used as comparative experimental data (Table 1). All children were scheduled for a selective dorsal rhizotomy to reduce spasticity in the legs. Based on clinical indication criteria,[20] participants were selected as having spasticity as the primary impairment affecting their gait, with coimpairments such as weakness and contracture playing a smaller role. Written informed consent was given by the parents as well as by children older than 12. The study protocol was approved by the medical ethics committee of the Amsterdam UMC, location VU Medical Centre.

Data were collected as part of clinical care between November 2015 and June 2019 by the gait lab clinicians. In a physical exam, spasticity levels were quantitatively assessed for the rectus femoris, hamstrings, gastrocnemius, and soleus using the Spasticity Test (SPAT).[21] In the SPAT, each muscle was manually stretched at a fast speed and one of the following scores allocated: 0 = no spasticity, 1 = an increase in muscle resistance somewhere in the range of motion, 2 = an increase in muscle resistance with a clear catch and a release, 3 = an increase in muscle resistance with a clear catch without release, 4 = clonus with less than 5 beats, and 5 = clonus with 5 beats or more.

In the same session, all children walked on an overground walkway at their self-chosen comfortable walking speed. Motion capture data were collected at 100 Hz using the Human Body Model marker set (Vicon).[22,23] Ground reaction forces (GRFs) were simultaneously collected at 1000 Hz using 2 (before March 2017) or 5 (from March 2017) embedded force plates (AMTI). Electromyography (EMG) data were recorded with bipolar sensors at 1000 Hz for the rectus femoris, vastus lateralis, semitendinosus, tibialis anterior, gastrocnemius medialis, and soleus muscles (Cometa). Two to 5 strides per leg of each child with a clean force plate hit were selected.

Gait data were analyzed using OpenSim (version 4.1, open-source software).[24] The gait 2392 musculoskeletal model[25] was scaled to each participant's proportions extracted from a static T-pose trial. OpenSim's inverse kinematic and inverse dynamic tools were used to compute joint angles and moments from walking trials,[24] and joint powers were calculated using angular velocities and moments using custom-written scripts in MATLAB 2016a (The MathWorks Inc). EMG signals were bandpass filtered between 30 and 300 Hz, full-wave rectified, and low-pass filtered by 6 Hz. Both filters were second-order recursive Butterworth filters. For visualization purposes, EMG waveforms were normalized to their highest value during the walking trial. All variables were time normalized to stride duration to have the same number of samples (ie, 101) for each stride.

Because of heterogeneity in the data, displayed by large SDs in kinematic and kinetic variables, a cluster analysis was performed to obtain representative subgroups of gait patterns per leg of the children included in this study. The *kmeans* algorithm was used in MATLAB 2016a, with experimental sagittal GRFs, joint (ie, hip, knee, and ankle) and foot to horizontal (foot pitch) angles, joint moments, and joint powers from each patient as input. The number of gait clusters was visually set when adding an extra cluster did not explain much more of the variance, also known as the elbow method (Appendix A). Averaged time-normalized GRFs, joint angles, moments and powers, and muscle excitations derived from EMG were calculated for each cluster. Furthermore, a Kruskal–Wallis test was performed on the SPAT scores of each muscle to test whether these scores were different between clusters.

Table 1 Patient Demographics and Gross Motor Function Classification System[19] Level

Diagnosis	14 CP, 3 HSP
Sex	9 boys, 8 girls
Age, y	8.2 (3.64) [4, 17]
Height, cm	132 (19) [108, 163]
Mass, kg	31 (14) [17, 64]
Gross Motor Function Classification System	4 × I, 13 × II

Abbreviations: CP, cerebral palsy; HSP, hereditary spastic paraplegia. Note: The values are presented as mean (SD) [minimum, maximum].

Nested Optimization

For each gait cluster, a nested optimization scheme was used to find velocity- or force-based hyperreflexia values that resulted in predictive simulations that best matched the experimental data (Figure 1). The inner loop ran predictive gait simulations, using hyperreflexia values that were set and optimized by the outer loop. Both loops are described next, starting with the inner loop, followed by the outer loop.

Inner Loop

The inner loop process used our previously developed forward dynamic simulation framework that showed good reproductions of typical gait[26] and idiopathic toe walking.[12] The simulations ran within Simulated Controller OptimizatioN Environment (SCONE)[27] with its Hyfydy model[28] based on an OpenSim model[25,29] with 9 muscles per leg and 2 viscoelastic contact spheres on the calcaneus and metatarsophalangeal joints of each foot.[30] Muscles were controlled by the reflex-based controller from Geyer and Herr[31] to which supraspinal drive was added.[26] Also, the control for the rectus femoris, hamstrings, gastrocnemius, and soleus muscles was expanded such that these muscles were controlled by length-, velocity-, and force-based reflexes and

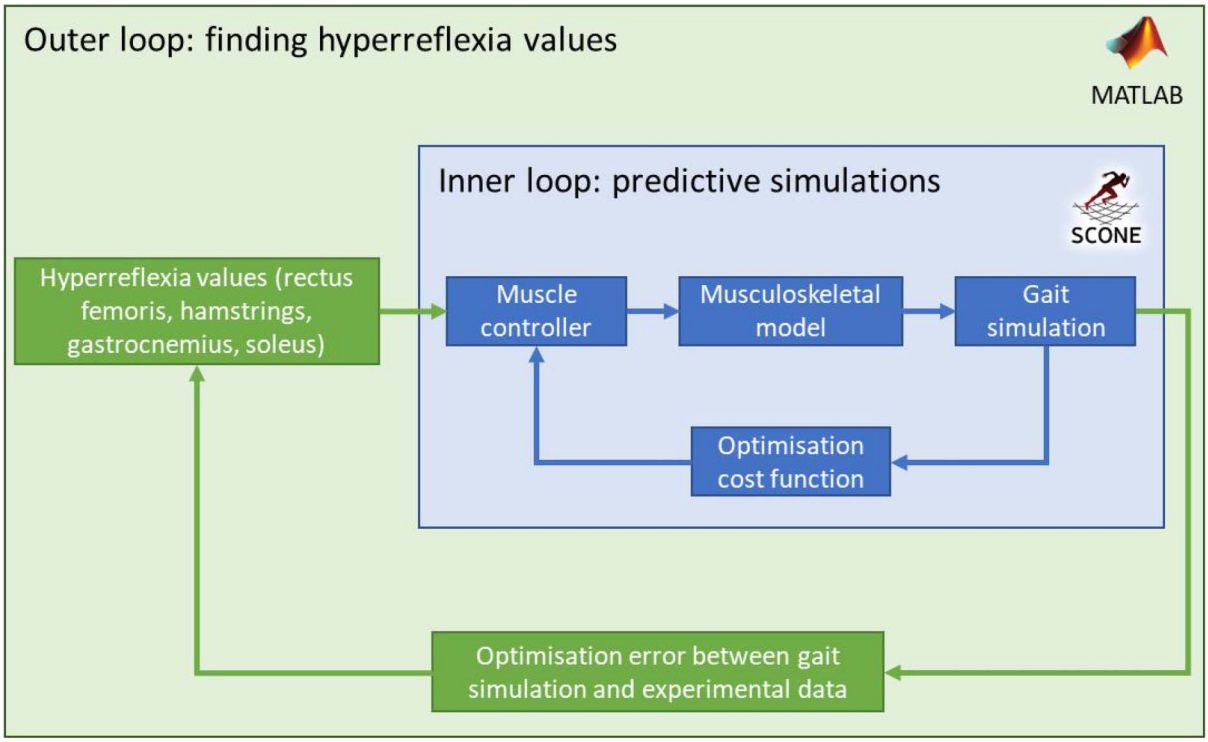

Figure 1 — Diagram of the nested optimization process to find hyperreflexia values that predict gait best matching experimental data. SCONE indicates Simulated Controller OptimizatioN Environment.

supraspinal drive, instead of only one type of reflex, to be more complete and realistic of spindles.[32,33] Hence, these muscle's excitations U were modeled according Equation 1:

$$U = C0 + \mathrm{GF} \times F + \mathrm{GL} \times L + \mathrm{GV} \times V. \quad (1)$$

In this, *C0* represents the supraspinal drive and GF, GL, and GV the reflex gains for the muscle force F, fiber length L, and fiber velocity V, respectively. Reflex delays were 10 milliseconds for the iliopsoas, rectus femoris, gluteus maximus, and hamstrings; 20 milliseconds for the vasti and biceps femoris short head; and 35 milliseconds for the tibialis anterior, gastrocnemius, and soleus.[34] The 160 design variables of the inner loop for a typical gait optimization consisted of the muscles' reflex gains and supraspinal drive values as well as the model's initial pose, which were optimized through a covariance matrix adaptation evolution strategy[35] on a 24-core Intel Xeon CPU E5-2690 2.60 GHz processor.

The multiobjective weighted cost function that was minimized in the inner loop consisted of cost of transport,[36] head stability, foot–ground impact, knee hyperextension, and muscle activation squared per distance travelled, as described in Veerkamp et al.[26] Also, a penalty was added that prevented muscle fibers from functioning on the descending limb of the force–length curve,[37] and normalized muscle activations above 0.9 were penalized to prevent unrealistic maximal activations. The duration of each simulation was set to 10 seconds, and walking speed was free to vary above 0.5 m/s. For each scenario, 12 separate optimizations were performed with different random seeds, using an initial SD of the design variables of 0.01. Optimizations stopped as soon as the cost function, averaged over the last 500 generations, did not improve more than 0.01% per generation. From the 12 optimizations, the simulation with the overall lowest cost function score was selected for subsequent quantitative evaluation. From this simulation, the first 2 gait cycles were excluded, and waveforms were time normalized and averaged over all subsequent gait cycles, which were typically all very similar. Muscle excitations were filtered by a 6-Hz low pass second-order Butterworth filter.

Hyperreflexia was modeled in the predictive simulations by increasing the optimized reflex gains from typical gait for the rectus femoris, hamstrings, gastrocnemius, and soleus muscles as these muscles were primarily affected in the patient groups. For each of these muscles, a single hyperreflexia value was added to the typical reflex gains across each gait phase for either of the velocity- or force-based reflexes as it was previously shown that spastic gait has similar reflex gain modulation as typical gait but at a higher amplitude.[6] The 20 reflex gains with hyperreflexia (ie, 4 muscles × 5 gait phases) were removed from the design variables of the inner loop optimization such that 140 design variables remained. As an initial guess for the optimization, the optimized parameters from a predictive simulation with slightly increased reflex gains were used (ie, 0.3 for velocity-based, 2 for force-based hyperreflexia). Hyperreflexia values were set by the outer loop.

Outer Loop

The outer loop of the nested optimization optimized the hyperreflexia values to get the best match with each cluster's experimental data. The root mean square errors (RMSE) between simulated and experimental sagittal hip, knee, and ankle angles and moments were minimized using a *surrogateopt* algorithm in MATLAB 2019b. Each RMSE was divided by its average experimental SD to enable comparisons of the RMSE between variables with different magnitudes. Hyperreflexia value constraints were 0 to 1 for velocity-based hyperreflexia and 0 to 20 for force-based hyperreflexia. In pilot simulations, it was found that values above the previously described upper bounds resulted in only a few

optimizations converging to a walking simulation in the inner loop, giving little confidence that actual optimums were found.

Evaluations of Optimization Results

For the gait predicted by each nested optimization for each gait cluster and each type of hyperreflexia, the match between the simulations and the experimental data was quantified using the coefficients of determination (R^2) and RMSE. These values were computed for different categories of biomechanical variables, that is, GRF, joint and foot pitch angles, joint moments, joint powers, and normalized muscle excitations. An average R^2 and RMSE were calculated by averaging the values over all variables. RMSE of the excitations were excluded as absolute amplitudes are difficult to compare when EMG is not normalized by maximum voluntary contractions, whereas the simulation excitation output was normalized to maximum voluntary contractions. The RMSE for each variable was divided by its average experimental SD. For each cluster, it was evaluated whether velocity- or force-based hyperreflexia best predicted experimental data based on R^2 and RMSE. This was done by calculating which type of hyperreflexia predicted most variables best. For each variable, the best performing type for each cluster was scored with a 1, the worst with a 0. The obtained distribution was compared against a distribution of 0.5 (ie, when both types of hyperreflexia would score equally) using a binomial test (IBM SPSS Statistics, version 20). Furthermore, the predicted walking speed of the simulations was compared with the average walking speed of each cluster.

For the modeled type of hyperreflexia that resulted in the best match with experimental data, the optimized values were compared for each muscle between clusters to evaluate which muscles were predominantly involved in each gait pattern. Furthermore, these values were compared against average SPAT scores to explore whether there was consistency between the simulations and experimental measures of each muscle's level of spasticity. Values were ranked within muscles (ie, sorted from low to high), and ranks between hyperreflexia and SPAT values were statistically compared by Spearman rho in SPSS per muscle and over all muscles.

Results

Three different gait clusters were found (Appendix A). The first cluster (14 legs) predominantly showed increased knee flexion during stance compared with typical gait. The second cluster (11 legs) showed increased hip and knee flexion at initial contact and some increased plantar flexion over the gait cycle. The third cluster (9 legs) showed increased knee flexion and substantial increased ankle plantar flexion throughout the gait cycle. SPAT scores differed between clusters for the hamstrings ($P = .035$) and soleus ($P = .004$), showed a trend for the gastrocnemius ($P = .077$), and were not significantly different for the rectus femoris ($P = .55$). For each cluster, the kinematics, kinetics, and muscle excitations from each nested optimization were predicted with varying levels of accuracy (Figures 2–4).

For the first cluster, the best velocity-based hyperreflexia simulation was close to the experimental data but did not show enough ankle dorsiflexion and showed too much knee extension in preswing. The best simulation with force-based hyperreflexia showed too much ankle plantar flexion and lacked increased knee flexion at initial contact, as present in the experimental data. In both simulations, the soleus excitation showed a double bump pattern, as present in the experimental data. The velocity-based hyperreflexia simulation (R^2: .63; RMSE: 1.42 SD; Figure 5) performed slightly better than the force-based hyperreflexia simulation (R^2: .63; RMSE: 1.63 SD). The walking speed of the velocity-based hyperreflexia simulation (1.01 m/s) was closer to the average experimental speed of this cluster (1.00 [0.24] m/s) than the force-based hyperreflexia simulation (1.25 m/s).

For the second cluster, both simulations showed a good prediction of the increased ankle plantar flexion. However, the velocity-based hyperreflexia simulation exhibited increased hip and knee flexion at initial contact, as present in the experimental data, whereas the force-based hyperreflexia simulation did not. Both simulations showed a soleus double bump excitation pattern and high gastrocnemius excitation instance, reflecting experimental data. The velocity-based hyperreflexia simulation also showed gastrocnemius activity in swing. The velocity-based hyperreflexia simulation (R^2: .66; RMSE: 1.19 SD) performed somewhat better than the force-based hyperreflexia simulation (R^2: .61; RMSE: 1.28 SD) for this cluster. The walking speed of the velocity-based hyperreflexia simulation (0.96 m/s) was closer to this cluster's average experimental speed (1.01 [0.18] m/s) than the force-based hyperreflexia simulation (1.10 m/s).

For the third cluster, both simulations matched the experimental kinematics well, with increased knee flexion at initial contact and increased plantar flexion over the gait cycle. The velocity-based hyperreflexia simulation did not show enough ankle plantar flexion during push off, which was better achieved by the force-based hyperreflexia simulation, although the plantar flexion timing was better for the velocity-based compared with the force-based hyperreflexia simulation. In the velocity-based hyperreflexia simulation, both the gastrocnemius and the soleus muscle did not show a clear excitation peak during push off and remained active in swing. In the experiment data, a clearer push-off excitation was visible, but the predicted soleus excitation in swing was in agreement with the experimental data. Overall, the velocity-based hyperreflexia simulation (R^2: .59; RMSE: 1.49 SD) performed slightly better than the force-based hyperreflexia simulation (R^2: .50; RMSE: 1.71 SD). The walking speed of the velocity-based hyperreflexia simulation (0.87 m/s) was closer to the average experimental speed of this cluster (0.85 [0.21] m/s) than the force-based hyperreflexia simulation (1.08 m/s).

Over all clusters, velocity-based hyperreflexia scored better than force-based hyperreflexia for 74% of the examined biomechanical variables (Figure 5), which was significantly different from a 50% distribution, as shown by the binomial distribution test ($P = .019$).

Optimized velocity-based hyperreflexia values for each cluster are shown in Figure 6A and Appendix B. Velocity-based hyperreflexia values for the first cluster were highest for the hamstrings and rectus femoris muscles. For the second cluster, hyperreflexia values were highest for the gastrocnemius, and for the third cluster, values were highest for the hamstrings, gastrocnemius, and soleus muscle. The rectus femoris and soleus showed a similar ranking of the experimental SPAT values (rho = 1). The hamstrings scored a rho of .5, and the gastrocnemius scored worst with a rho of −.5. Overall, Spearman rho between optimized and experimental values was .5 ($P = .098$).

Discussion

This study aimed to evaluate the pathophysiological mechanisms underlying gait deviations seen in children with spastic paresis,

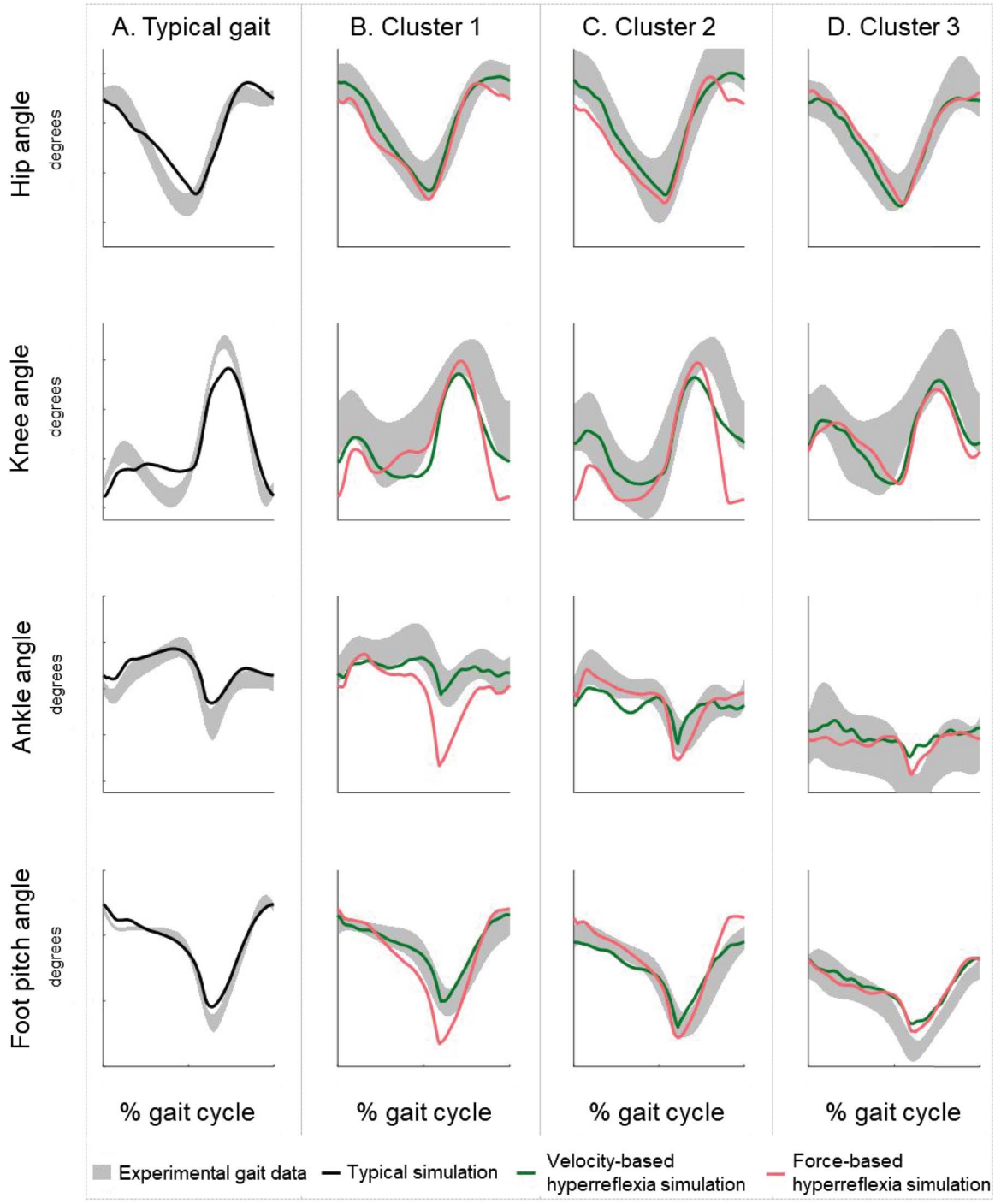

Figure 2 — Predicted kinematics for (A) typical gait and for gait patterns from children with spasticity, that is, (B) cluster 1 with mostly increased knee flexion during stance, (C) cluster 2 with mostly increased ankle plantar flexion, and (D) cluster 3 with increased knee flexion and ankle plantar flexion. For each of the gait patterns, velocity- and force-based hyperreflexia were imposed, separately. Experimental kinematics display ± 1 SD from the mean. Comparative experimental data for typical gait were obtained as described in Veerkamp et al.[26]

characterized predominantly by spasticity. Three clusters of gait patterns emerged, with distinct differences in knee and ankle kinematics throughout the gait cycle. Velocity-based hyperreflexia predicted spastic gait patterns better than force-based hyperreflexia. Each gait pattern was explained by different combinations of spasticity between muscles, with some similarities between the relative contributions of spastic muscles within the simulations and experimentally measured spasticity scores. These insights into the role of spastic muscles in gait can guide clinical recognition of when and where spasticity is present and may inform targeted treatment.

Most gait deviations and some SPAT score ranks could be predicted by the simulations, suggesting that spasticity could, indeed, be the predominant impairment affecting gait in the

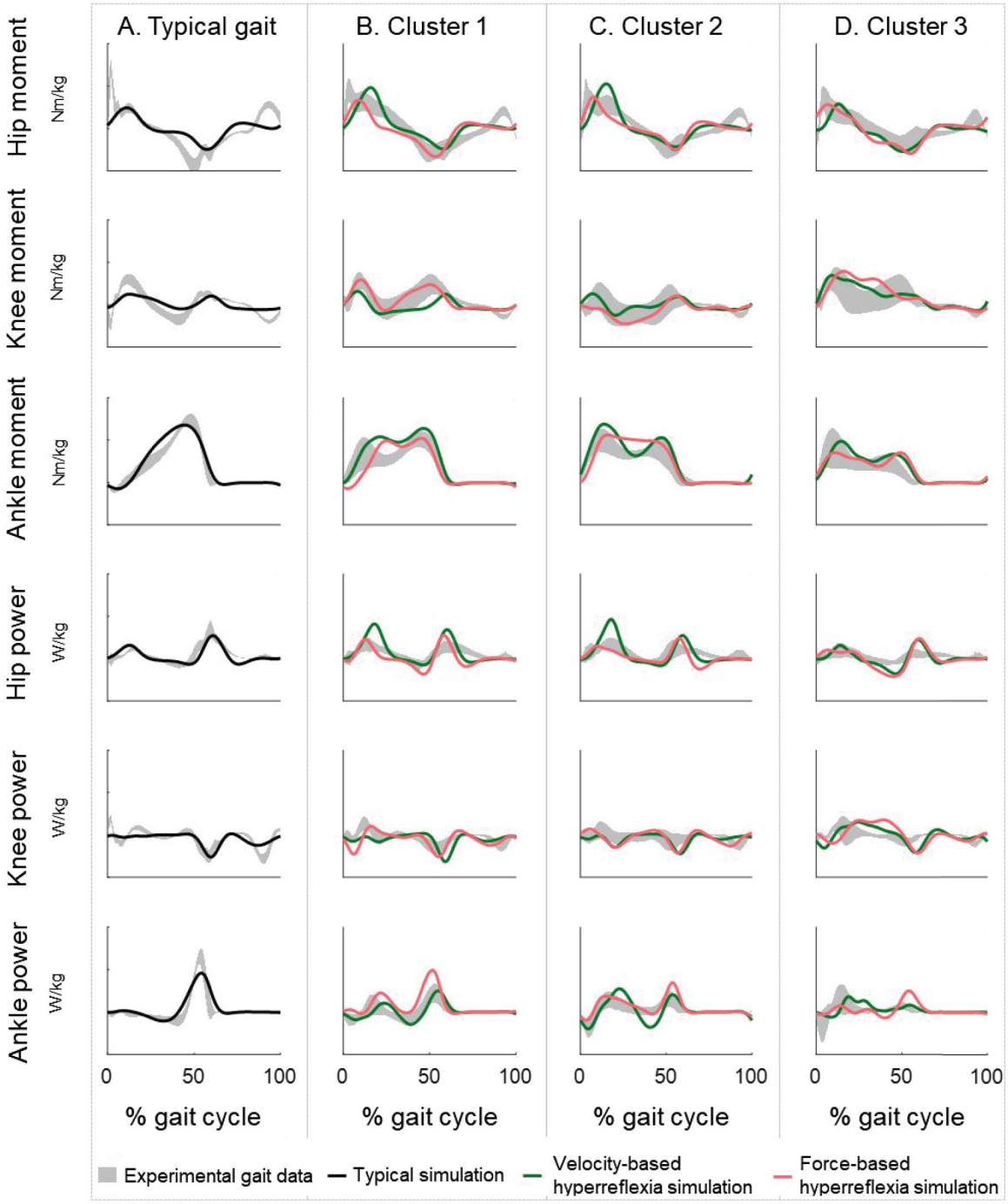

Figure 3 — Predicted kinetics for (A) typical gait and for gait patterns from children with spasticity, that is, (B) cluster 1 with mostly increased knee flexion during stance, (C) cluster 2 with mostly increased ankle plantar flexion, and (D) cluster 3 with increased knee flexion and ankle plantar flexion. For each of the gait patterns, velocity- and force-based hyperreflexia were imposed, separately. Experimental kinematics display ±1 SD from the mean. Comparative experimental data for typical gait were obtained as described in Veerkamp et al.[26]

selected children. However, some differences between predicted and experimental gait still existed, and optimized and experimental spasticity values for the gastrocnemius did not match well. Perhaps, besides spasticity, other impairments also contribute to the gait deviations in the experimental gait patterns that may explain the observed differences. The simulation predicting the first cluster with increased knee flexion predominantly showed spastic involvement of the rectus femoris and hamstrings, whereas during the physical exam, spasticity was also detected in the gastrocnemius and soleus in children within this cluster. These children may have also presented with plantar flexor muscle weakness, which is often present in CP[39–42] but was not modeled in this study nor measured within our patient group. Perhaps, plantar flexor spasticity would have resulted in increased plantar flexion during gait in these children, but this could be neutralized by weakness. Furthermore, in the third gait pattern, with increased knee flexion and ankle

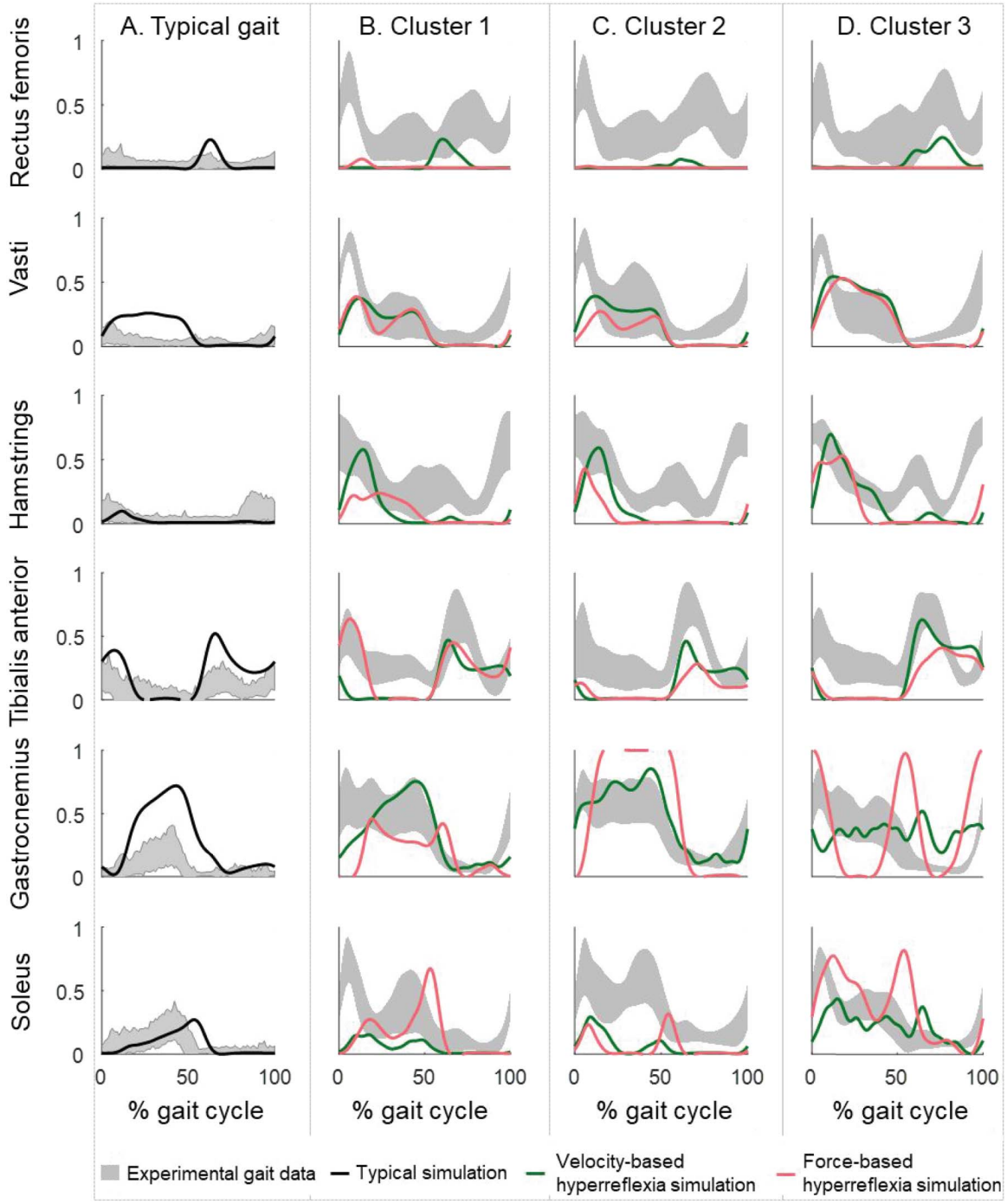

Figure 4 — Predicted normalized muscle excitations for (A) typical gait and for gait patterns from children with spasticity, that is, (B) cluster 1 with mostly increased knee flexion during stance, (C) cluster 2 with mostly increased ankle plantar flexion, and (D) cluster 3 with increased knee flexion and ankle plantar flexion. For each of the gait patterns, velocity- and force-based hyperreflexia were imposed, separately. Experimental kinematics display ±1 SD from the mean. Comparative experimental data for typical gait were obtained from Bovi et al.[38]

plantar flexion, a prominent difference between the simulation and the experimental data was the lack of increasing ankle plantar flexion during push off in the simulation. Further assessment of the physical exam data (Appendix C) revealed that these children also had limited ankle range of motion (maximum dorsiflexion angle of −5° [12°] with knee flexed, −12° [8°] with knee extended), which was not modeled. Therefore, within the simulation, the plantar flexors may be performing at such short normalized fiber lengths during push off that further plantar flexion could not be achieved, whereas further plantar flexion may have been possible when the contracture was also modeled.

Even though the optimized hyperreflexia values and experimental SPAT scores generally showed some similarities across clusters, it needs to be noted that the comparative value of the

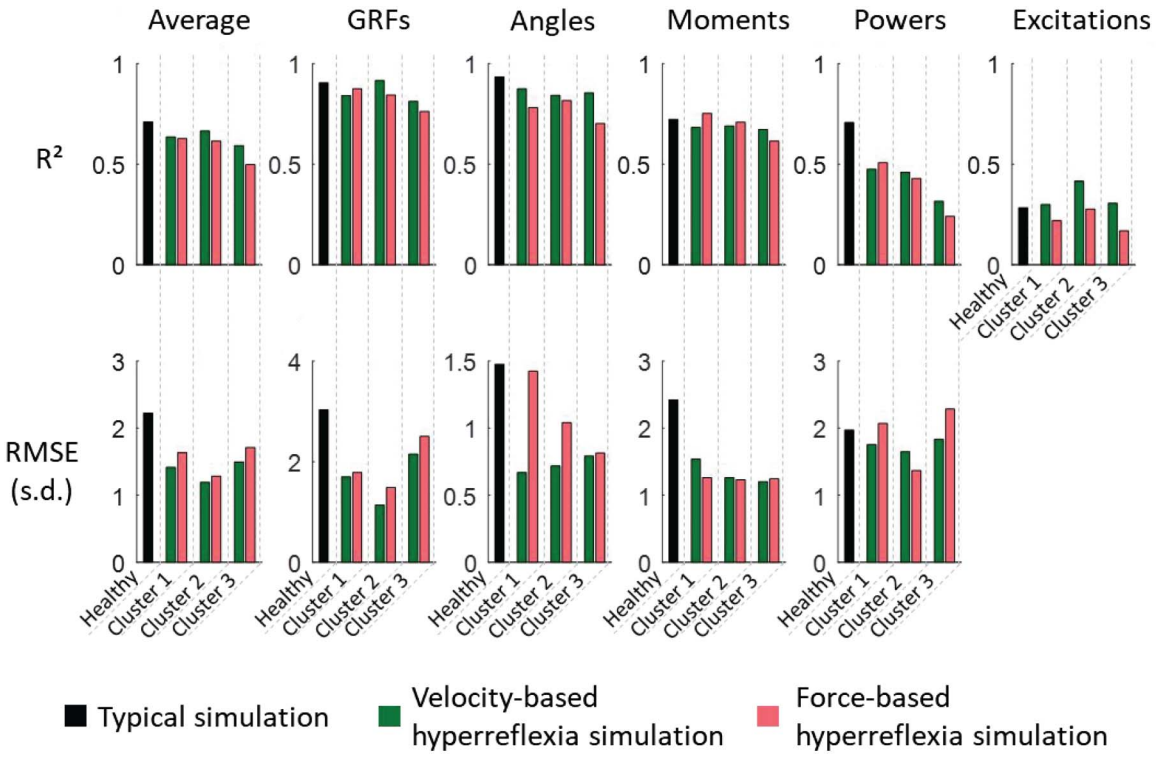

Figure 5 — Matches for each of the predictive simulations with the corresponding experimental data (ie, experimental data of typical gait or of one of the clusters), quantified by the coefficient of determination (R^2) and RMSE for different biomechanical categories as well as averaged over all categories. GRFs indicates ground reaction forces; RMSE, root mean square errors.

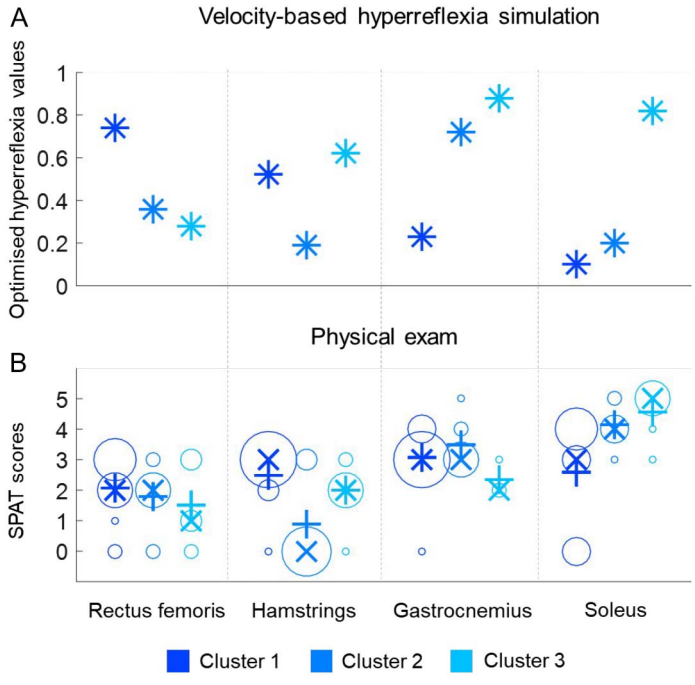

Figure 6 — Spasticity scores for the rectus femoris, hamstrings, gastrocnemius, and soleus muscles for each cluster as (A) optimized within the predictive simulations with velocity-based hyperreflexia (displayed by *) and (B) as measured during a physical exam by the SPAT (median displayed by ×, mean displayed by +; the size of the circles indicates the distribution of the individual data points: a bigger circle means that that value was measured in more patients). SPAT indicates Spasticity Test.

SPAT score is limited. It has been shown that the SPAT also correlates with tissue stiffness,[43] indicating that it is difficult to distinguish neural and nonneural contributors to joint resistance by such a manual assessment. Instead, an instrumented spasticity assessment, such as described by van Den Noort et al[44] and Bar-On et al,[45] could be used to quantify neural hyperreflexia and may provide a more valid comparison. Unfortunately, such assessment was not performed within our patient group. However, even when using such an instrumented spasticity assessment, comparisons would not be completely valid. Hyperreflexia gains in passive and active conditions are not necessarily interchangeable,[46] and reflex gains have been shown to be task dependent.[47,48]

The finding that modeling velocity-based hyperreflexia can predict experimental data from children with spasticity is in agreement with most simulation studies.[13–15] However, Bruel et al,[15] Jansen et al,[14] and Falisse et al[16] changed length-based reflex gains simultaneously with velocity-based hyperreflexia. We chose not to add length-based hyperreflexia as it would double the number of hyperreflexia values to be optimized, and pilot simulations showed only a minor additional effect from length-based hyperreflexia. Jansen et al[14] also mentioned a minor difference between length hyperreflexia and velocity hyperreflexia. Moreover, Bar-On et al[18] showed that most spastic muscles were predominantly sensitive to velocity changes, rather than length changes, during passive stretches.

Our study findings contrast with the findings of Falisse et al,[16] who showed that force-based hyperreflexia outperformed velocity-based hyperreflexia in predicting muscle activations during gait of children with CP. Differences in modeling approach and patient selection may explain this contradicting finding. Falisse et al also modeled force-derivate feedback, whereas we chose not to do this

as this derivative is very sensitive to noise. Also, the spasticity model in Falisse et al was fitted to the passive stretch experimental data and not to gait, whereas, as mentioned, passive and active hyperreflexia gains may not be the same. Furthermore, the simulations from Falisse et al were not fully predictive but required EMG and musculotendon lengths as input, which could have been affected by other neuromusculoskeletal impairments. Moreover, such other impairments may be playing a bigger role in the children selected by Falisse et al as these children were not specifically selected based on spasticity being their primary impairment. Nevertheless, it may also be that spasticity can be explained by a combination of velocity- and force-based hyperreflexia. For example, for the first cluster, the force-based hyperreflexia simulation predicts increased knee flexion in preswing, which the velocity-based hyperreflexia could not achieve, suggesting how they could complement each other. Nonetheless, testing combinations of hyperreflexia types is computationally expensive as the number of hyperreflexia values that needs to be optimized by the outer loop increases. Each nested optimization in the current study took around 5 days, and it would have been prohibitive to further increase simulation times.

Within neurophysiological literature, there is a stronger base of evidence for spasticity being a velocity-dependent phenomenon as opposed to force dependent.[49,50] The source of spasticity is suggested to be disinhibition of feedback from the muscle spindles within the spinal cord.[51] Even though a recent paper has suggested that spindle firing depends on force and force derivative,[17] this does not seem to weigh up against evidence for spindle sensitivity to length and velocity (eg, Matthews and Stein[33]; Matthews[32]). Length, velocity, and force are possibly also correlated in many experimental conditions, challenging studies of the underlying physiological mechanisms. It may be that in spasticity, inhibition of the Ia afferents from the spindles, which provide velocity feedback, is suppressed,[18,52] but the exact physiological mechanism of velocity dependency of spasticity remains unclear.[53]

Several limitations and assumptions of this study need to be considered in interpreting the findings of our simulation study. First, we used a 2D (sagittal) model, whereas muscles prone to spasticity also contribute to gait deviations in the frontal and transverse planes. Further developments in the controller are required to enable evaluation of effects of spasticity in 3D, for example, by also being able to include adductor and tibialis posterior spasticity. Second, hyperreflexia values were added to typical reflex gains, but these typical gains could not be validated. Third, our framework used a cost function that was tuned to predict typical gait.[26] For children with CP, the criteria may be weighted differently, and other factors, such as pain, may also play a role. Fourth, some children did show limited joint range of motion, particularly in the ankle (Appendix C), which likely also affected their gait. Fifth, walking speed was free to vary within the simulations, and the force-based hyperreflexia simulations resulted in a faster walking speed than experimentally found for each cluster. The velocity-based hyperreflexia simulations predicted a closely matching walking speed. Therefore, the force-based simulation's worse match with experimental biomechanical variables may be explained by differences in walking speed. However, we preferred not to impose the simulation's walking speed as this would limit the framework's applicability in predicting gait for new situations in which the walking speed is unknown. Furthermore, it may be considered a strong result from the velocity-based hyperreflexia simulations that experimental walking speed was predicted closely.

This study has provided insights into the role of spastic muscles in different gait patterns. These insights can guide clinical recognition of when and where spasticity is present in a patient. The cause-and-effects mechanisms of how spasticity affects gait could be used to verify relations between gait deviations and impairments. Such relations are used in clinical practice to guide treatment selection.[54–56] As a next step, spasticity should be combined with other impairments, such as weakness and contracture, to elucidate the interaction of these impairments. This may assist in the clinical reasoning process of gait analysis interpretation in children with CP and other neuromuscular disorders, which could improve treatment selection. Combining impairments would also be important for patient-specific simulation, which can account for the heterogeneity within the population. Moreover, the effects of interventions can be investigated and validated with postintervention gait data. Combined, this would be a step toward the ultimate goal of being able to use patient-specific predictive simulations to predict and optimize treatment outcomes.

In conclusion, we have shown that different gait patterns of children with spasticity can be distinguished. Each of these gait patterns can be predicted reasonably by simulations with velocity-based hyperreflexia, and each gait pattern was explained by a different combination of spastic muscles.

References

1. Cans C. Surveillance of cerebral palsy in Europe: a collaboration of cerebral palsy surveys and registers. *Dev Med Child Neurol*. 2000;42(12):816–824. doi:10.1111/j.1469-8749.2000.tb00695.x
2. Oskoui M, Coutinho F, Dykeman J, Jetté N, Pringsheim T. An update on the prevalence of cerebral palsy: a systematic review and meta-analysis. *Dev Med Child Neurol*. 2013;55(6):509–519. doi:10.1111/dmcn.12080
3. Fink JK. Hereditary spastic paraplegia: clinico-pathologic features and emerging molecular mechanisms. *Acta Neuropathol*. 2013;126(3):307–328. doi:10.1007/s00401-013-1115-8
4. Lance J. Pathophysiology of spasticity and clinical experience with baclofen. In: Lance J, Feldman R, Young R, & Koella W, eds. *Spasticity: Disordered Motor Control*. Symposia Specialists; 1980:185–204.
5. van den Noort JC, Bar-On L, Aertbeliën E, et al. European consensus on the concepts and measurement of the pathophysiological neuromuscular responses to passive muscle stretch. *Eur J Neurol*. 2017;24(7):981-e38. doi:10.1111/ene.13322
6. Hodapp M, Klisch C, Mall V, Vry J, Berger W, Faist M. Modulation of soleus H-reflexes during gait in children with cerebral palsy. *J Neurophysiol*. 2007;98(6):3263–3268. doi:10.1152/jn.00471.2007
7. Jaspers E, Verhaegen A, Geens F. Lower limb functioning and its impact on quality of life in ambulatory children with cerebral palsy. *Eur J Paediatr Neurol*. 2013;17(6):561–567. doi:10.1016/j.ejpn.2013.04.006
8. Novak I, Morgan C, Fahey M, et al. State of the evidence traffic lights 2019: systematic review of interventions for preventing and treating children with cerebral palsy. *Curr Neurol Neurosci Rep*. 2020;20(2):1022. doi:10.1007/s11910-020-1022-z
9. Novak I, Mcintyre S, Morgan C, et al. A systematic review of interventions for children with cerebral palsy: state of the evidence. *Dev Med Child Neurol*. 2013;55(10):885–910. doi:10.1111/dmcn.12246
10. Ong CF, Geijtenbeek T, Hicks JL, Delp SL. Predicting gait adaptations due to ankle plantarflexor muscle weakness and contracture

using physics-based musculoskeletal simulations. *PLoS Comput Biol*. 2019;15(10):e1006993. doi:10.1371/journal.pcbi.1006993
11. Waterval NFJ, Veerkamp K, Geijtenbeek T, et al. Validation of forward simulations to predict the effects of bilateral plantarflexor weakness on gait. *Gait Posture*. 2021;87:33–42. doi:10.1016/j.gaitpost.2021.04.020
12. Veerkamp K, van der Krogt MM, Waterval NFJ, et al. Predictive simulations identify potential neuromuscular contributors to idiopathic toe walking. 2023.
13. van der Krogt MM, Bar-On L, Kindt T, Desloovere K, Harlaar J. Neuro-musculoskeletal simulation of instrumented contracture and spasticity assessment in children with cerebral palsy. *J Neuroeng Rehabil*. 2016;13(1):64. doi:10.1186/s12984-016-0170-5
14. Jansen K, De Groote F, Aerts W, De Schutter J, Duysens J, Jonkers I. Altering length and velocity feedback during a neuro-musculoskeletal simulation of normal gait contributes to hemiparetic gait characteristics. *J Neuroeng Rehabil*. 2014;11(1):78. doi:10.1186/1743-0003-11-78
15. Bruel A, Ghorbel SB, Di Russo A, et al. Investigation of neural and biomechanical impairments leading to pathological toe and heel gaits using neuromusculoskeletal modelling. *J Physiol*. 2022;600(11):2691–2712. doi:10.1113/JP282609
16. Falisse A, Bar-On L, Desloovere K, Jonkers I, De Groote F. A spasticity model based on feedback from muscle force explains muscle activity during passive stretches and gait in children with cerebral palsy. *PLoS One*. 2018;13(12):e0208811. doi:10.1371/journal.pone.0208811
17. Blum KP, Lamotte D'Incamps B, Zytnicki D, Ting LH. Force encoding in muscle spindles during stretch of passive muscle. *PLoS Comput Biol*. 2017;13(9):e1005767. doi:10.1371/journal.pcbi.1005767
18. Bar-On L, Aertbeliën E, Molenaers G, Desloovere K. Muscle activation patterns when passively stretching spastic lower limb muscles of children with cerebral palsy. *PLoS One*. 2014;9(3):e91759. doi:10.1371/journal.pone.0091759
19. Rosenbaum PL, Walter SD, Hanna SE, et al. Prognosis for gross motor function in cerebral palsy: creation of motor development curves. *J Am Med Assoc*. 2002;288(11):1357–1363. doi:10.1001/jama.288.11.1357
20. Oudenhoven LM, van der Krogt MM, Romei M, et al. Factors associated with long-term improvement of gait after selective dorsal rhizotomy. *Arch Phys Med Rehabil*. 2019;100(3):474–480. doi:10.1016/j.apmr.2018.06.016
21. Scholtes VA, Dallmeijer AJ, Becher JG. The Spasticity Test: a clinical instrument to measure spasticity in children with cerebral palsy. In: Ponsen & Looijen BV, ed. *The Effectiveness of Multilevel Botulinum Toxin Type A and Comprehensive Rehabilitation in Children with Cerebral Palsy*. Wageningen; 2007:29–64.
22. van den Bogert AJ, Geijtenbeek T, Even-Zohar O, Steenbrink F, Hardin EC. A real-time system for biomechanical analysis of human movement and muscle function. *Med Biol Eng Comput*. 2013;51(10):1069–1077. doi:10.1007/s11517-013-1076-z
23. Flux E, van der Krogt MM, Cappa P, Petrarca M, Desloovere K, Harlaar J. The human body model versus conventional gait models for kinematic gait analysis in children with cerebral palsy. *Hum Mov Sci*. 2020;70:102585. doi:10.1016/j.humov.2020.102585
24. Seth A, Hicks JL, Uchida TK, et al. OpenSim: simulating musculoskeletal dynamics and neuromuscular control to study human and animal movement. *PLoS Comput Biol*. 2018;14(7):e1006223. doi:10.1371/journal.pcbi.1006223
25. Delp SL, Loan JP, Hoy MG, Zajac FE, Topp EL, Rosen JM. An interactive graphics-based model of the lower extremity to study orthopaedic surgical procedures. *IEEE Trans Biomed Eng*. 1990;37(8):757–767. doi:10.1109/10.102791
26. Veerkamp K, Waterval NFJ, Geijtenbeek T, et al. Evaluating cost function criteria in predicting healthy gait. *J Biomech*. 2021;123:110530. doi:10.1016/j.jbiomech.2021.110530
27. Geijtenbeek T. SCONE: open source software for predictive simulation of biological motion. *J Open Source Softw*. 2019;4(38):1421. doi:10.21105/joss.01421
28. Geijtenbeek T. The Hyfydy Simulation Software. 2021. https://Hyfydy.com.
29. Delp SL, Anderson FC, Arnold AS, et al. OpenSim: open-source software to create and analyze dynamic simulations of movement. *IEEE Trans Biomed Eng*. 2007;54(11):1940–1950. doi:10.1109/TBME.2007.901024
30. Hunt K, Crossley E. Coefficient of restitution interpreted as damping in vibroimpact. *J Appl Mech Am Soc Mech Eng*. 1975;42(2):440–445. doi:10.1115/1.3423596
31. Geyer H, Herr H. A muscle-reflex model that encodes principles of legged mechanics produces human walking dynamics and muscle activities. *IEEE Trans Neural Syst Rehabil Eng*. 2010;18(3):263–273. doi:10.1109/TNSRE.2010.2047592
32. Matthews PBC. The response of de-efferented muscle spindle receptors to stretching at different velocities. *J Physiol*. 1963;168(3):660–678. doi:10.1113/jphysiol.1963.sp007214
33. Matthews BPBC, Stein RB. The sensitivity of muscle spindle afferents to small sinusoidal changes of length. *J Physiol*. 1969;200(3):723–743. doi:10.1113/jphysiol.1969.sp008719
34. Frijns CJM, Laman DM, Van Duijn MAJ, Van Duijn H. Normal values of patellar and ankle tendon reflex latencies. *Clin Neurol Neurosurg*. 1997;99(1):31–36. doi:10.1016/S0303-8467(96)00593-8
35. Hansen N, Müller SD, Koumoutsakos P. Reducing the time complexity of the derandomized evolution strategy with covariance matrix adaptation (CMA-ES). *Evol Comput*. 2003;11(1):970. doi:10.1162/106365603321828970
36. Uchida TK, Hicks JL, Dembia CL, Delp SL. Stretching your energetic budget: how tendon compliance affects the metabolic cost of running. *PLoS One*. 2016;11(3):150378.
37. Harkness-Armstrong C, Maganaris C, Walton R, et al. (2021). In vivo operating lengths of the gastrocnemius muscle during gait in children who idiopathically toe-walk. *Exp Physiol*. 2022;107(12):1521–1524.
38. Bovi G, Rabuffetti M, Mazzoleni P, Ferrarin M. A multiple-task gait analysis approach: kinematic, kinetic and EMG reference data for healthy young and adult subjects. *Gait Posture*. 2011;33(1):6–13. doi:10.1016/j.gaitpost.2010.08.009
39. Graham HK, Rosenbaum P, Paneth N, et al. Cerebral palsy. *Nat Rev Dis Prim*. 2016;2(1):15082. doi:10.1038/nrdp.2015.82
40. Barber L, Barrett R, Lichtwark G. Medial gastrocnemius muscle fascicle active torque-length and Achilles tendon properties in young adults with spastic cerebral palsy. *J Biomech*. 2012;45(15):2526–2530. doi:10.1016/j.jbiomech.2012.07.018
41. Barrett RS, Lichtwark GA. Gross muscle morphology and structure in spastic cerebral palsy: a systematic review. *Dev Med Child Neurol*. 2010;52(9):794–804. doi:10.1111/j.1469-8749.2010.03686.x
42. Wiley ME, Damiano DL. Lower-extremity strength profiles in spastic cerebral palsy. *Dev Med Child Neurol*. 1998;40(2):100–107. doi:10.1111/j.1469-8749.1998.tb15369.x
43. De Gooijer-Van De Groep KL, De Vlugt E, De Groot JH, et al. Differentiation between non-neural and neural contributors to ankle joint stiffness in cerebral palsy. *J Neuroeng Rehabil*. 2013;10(1):81. doi:10.1186/1743-0003-10-81
44. van den Noort JC, Scholtes VA, Becher JG, Harlaar J. Evaluation of the catch in spasticity assessment in children. *Arch Phys Med Rehabil*. 2010;91(4):615–623. doi:10.1016/j.apmr.2009.12.022

45. Bar-On L, Aertbeliën E, Wambacq H, et al. A clinical measurement to quantify spasticity in children with cerebral palsy by integration of multidimensional signals. *Gait Posture*. 2013;38(1):141–147. doi:10.1016/j.gaitpost.2012.11.003
46. Crenna P. Spasticity and "spastic" gait in children with cerebral palsy. *Neurosci Biobehav Rev*. 1998;22(4):571–578. doi:10.1016/S0149-7634(97)00046-8
47. Zehr EP, Stein RB. What functions do reflexes serve during human locomotion? *Prog Neurobiol*. 1999;58(2):185–205. doi:10.1016/S0301-0082(98)00081-1
48. Schneider C, Lavoie BA, Capaday C. On the origin of the soleus H-reflex modulation pattern during human walking and its task-dependent differences. *J Neurophysiol*. 2000;83(5):2881–2890. doi:10.1152/jn.2000.83.5.2881
49. Powers RK, Campbell DL, Rymer WZ. Stretch reflex dynamics in spastic elbow flexor muscles. *Ann Neurol*. 1989;25(1):32–42. doi:10.1002/ana.410250106
50. Burke D, Gillies JD, Lance JW. The quadriceps stretch reflex in human spasticity. *J Neurol Neurosurg Psychiatry*. 1970;33(2):216–223. doi:10.1136/jnnp.33.2.216
51. Trompetto C, Marinelli L, Mori L, et al. Pathophysiology of spasticity: implications for neurorehabilitation. *Biomed Res Int*. 2014;2014:906. doi:10.1155/2014/354906
52. Sheean G. Neurophysiology of spasticity. In: Barnes MP, Johnson GR, eds. *Upper Motor Neurone Syndrome and Spasticity*. Cambridge University Press; 2008:9–54.
53. Sloot LH, Weide G, van der Krogt MM, et al. Applying stretch to evoke hyperreflexia in spasticity testing: velocity vs. acceleration. *Front Bioeng Biotechnol*. 2021;8:591004. doi:10.3389/fbioe.2020.591004
54. Sangeux M, Armand S. Kinematic deviations in children with cerebral palsy. *Orthopedic Management of Children With Cerebral Palsy*. Springer; 2015:241–253.
55. Zhou J, Butler EE, Rose J. Neurologic correlates of gait abnormalities in cerebral palsy: implications for treatment. *Front Hum Neurosci*. 2017;11:103. doi:10.3389/fnhum.2017.00103
56. van der Krogt MM, Houdijk H, Wishaupt K, van Hutten K, Dekker S, Buizer AI. Development of a core set of gait features and their potential underlying impairments to assist gait data interpretation in children with cerebral palsy. *Front Hum Neurosci*. 2022;16:907565. doi:10.3389/fnhum.2022.907565

Appendix A: Cluster Analysis Elbow Method

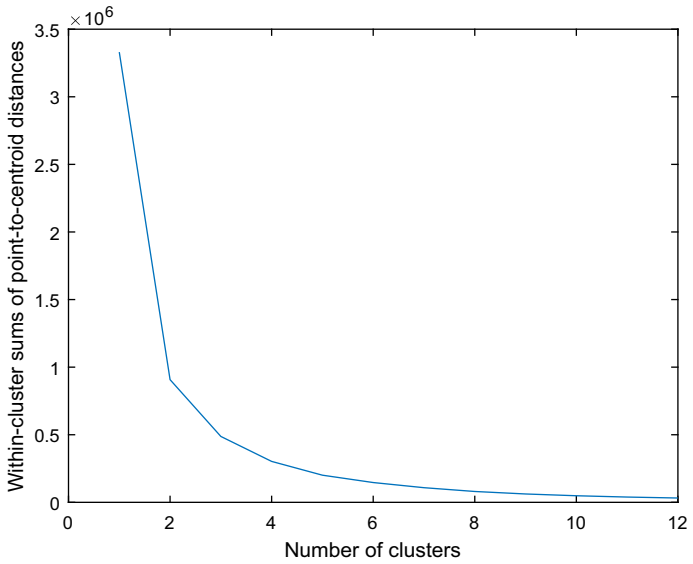

Figure A1 — The elbow method was used to visually determine the optimal number of clusters present in the experimental data. In this method, a number of clusters is selected to which adding an extra one does not explain much more of the variance. Based on this figure, the use of 3 clusters was considered to be optimal. This also made most sense when visually assessing the data as it resulted in gait patterns with clearly distinct gait patterns, with a quite even distribution of legs between cluster (9–14 legs per cluster).

Appendix B: Optimized Hyperreflexia Values

Table B1 Optimized Velocity-Based Hyperreflexia Values for Each Muscle and Each Cluster

	Rectus femoris	Hamstrings	Gastrocnemius	Soleus
Cluster 1	0.74	0.52	0.23	0.10
Cluster 2	0.36	0.19	0.72	0.20
Cluster 3	0.28	0.62	0.88	0.82

Table B2 Optimized Force-Based Hyperreflexia Values for Each Muscle and Each Cluster

	Rectus femoris	Hamstrings	Gastrocnemius	Soleus
Cluster 1	0	0.05	0.14	2.19
Cluster 2	6.73	2.19	20	2.93
Cluster 3	3.17	2.69	13.25	7.97

Appendix C: Joint Range of Motion per Cluster

	Cluster 1		Cluster 2		Cluster 3	
	Mean	SD	Mean	SD	Mean	SD
Supine						
Hip flexion	108.9	6.8	114.1	11.1	108.9	10.2
Hip abduction (knee flexed)	37.9	7.8	43.6	11.6	43.9	16.0
Hip abduction (knee extended)	20.4	4.1	28.2	7.8	25.0	9.0
Hip adduction	17.9	6.7	26.4	11.0	26.1	5.5
Knee flexion	142.1	13.0	146.4	11.6	148.9	7.8
Knee extension	−2.5	7.0	0.5	5.2	−2.8	5.7
Popliteal angle	71.8	7.5	65.9	20.0	65.0	16.8
Ankle plantarflexion	43.9	9.2	41.8	10.1	46.1	10.2
Ankle dorsiflexion (knee flexed)	6.4	6.0	5.0	13.6	−5.0	12.7
Ankle dorsiflexion (knee extended)	−2.5	7.0	0.5	12.5	−12.2	7.5
Prone						
Hip extension	5.0	11.3	−1.8	5.1	0.0	5.0
Hip endorotation	59.6	13.1	67.7	13.3	60.6	9.8
Hip exorotation	20.0	8.3	15.9	4.9	19.4	8.5
Knee flexion	109.6	27.0	121.8	19.9	121.1	20.3
Ankle varus	13.8	4.8	15.0	5.9	17.2	7.9
Ankle valgus	1.7	2.5	4.5	4.2	3.9	3.3
Ankle pronation	21.7	8.6	25.0	4.7	25.0	7.1
Ankle supination	29.6	16.8	32.5	17.8	33.1	11.9